Microfluid Nanofluid
DOI 10.1007/s10404-006-0117-4

RESEARCH PAPER

Simulations of complex particle transport in heterogeneous active liquids

Daphne Weihs · Michael A. Teitell · Thomas G. Mason

Received: 22 May 2006 / Accepted: 24 August 2006

Abstract Thermal-fluctuation and external force-induced motion of particles provide mechanical and rheological information for viscoelastic liquids and soft solids. Although particle tracking is well-developed, analysis of particle trajectories in active heterogeneous materials, such as living cells, is usually not simple or straightforward. These trajectories are sometimes composed of several concurrent processes occurring simultaneously or episodically in a complex fluid. Here, we introduce simulations that generate 2-dimensional trajectories of probe transport in a viscous liquid as a tool for complex-trajectory analysis. These computer simulations illustrate cases that are physically relevant and highlight key features, such as spatial confinements or convective speeds, which can for example define a cell's internal structure and active transport along tubules or fibers. Comparison to experimental data will allow quantitative identification of various concurrent processes and understanding of their time dependence. We examine several well-defined cases of particle motion that occur in soft samples, including living cells, and present information from the analysis as well as new approaches for complex processes.

Keywords Bio-microrheology · Brownian motion · Particle tracking · Mean square displacement

D. Weihs · M. A. Teitell
Department of Pathology and Laboratory Medicine, University of California at Los Angeles, Los Angeles CA 90095, USA

D. Weihs · M. A. Teitell (✉)
Institute for Cell Mimetic Space Exploration, University of California at Los Angeles, Los Angeles, CA 90095, USA
e-mail: mteitell@mednet.ucla.edu

M. A. Teitell · T. G. Mason
California NanoSystems Institute, University of California at Los Angeles, Los Angeles, CA 90095, USA

T. G. Mason
Department of Chemistry and Biochemistry, University of California at Los Angeles, Los Angeles, CA 90095, USA
e-mail: mason@chem.ucla.edu

T. G. Mason
Department of Physics and Astronomy, University of California at Los Angeles, Los Angeles, CA 90095, USA

D. Weihs (✉)
Faculty of Biomedical Engineering, Technion—Israel Institute of Technology, Haifa 32000, Israel
e-mail: daphnew@tx.technion.ac.il

1 Introduction

Particle tracking has recently become an invaluable tool for studying the transport and velocimetry in live cells, complex liquids, and soft solids (Qian et al. 1991; Crocker and Grier 1996). Particle tracking has been used to monitor thermally-induced, or "passive" motion (Mason and Weitz 1995; Mason et al. 1997a; Gittes et al. 1997) and forced, or actively manipulated particle motion (Evans et al. 1995) within soft materials in order to characterize liquid and solid-like phases. Specifically, particle-tracking microrheology has facilitated physical and mechanical characterization of heterogeneous microenvironments (Valentine et al. 2001). Non-perturbing, passive studies provide local

rheological and transport properties of complex liquids and soft solids (Mason and Weitz 1995; Crocker and Grier 1996; Mason 2000), while active manipulation probes mechano-structural properties of stiffer materials (Evans et al. 1995; Bausch et al. 1998). Microrheological, particle tracking methods have been adapted to study bio-molecules (Apgar et al. 2000; Salman et al. 2002; Gardel et al. 2003) and live cells (Bausch et al. 1999; Feneberg et al. 2001; Yamada et al. 2002; Bursac et al. 2005) as well as complex liquids (Xu et al. 1998; Weeks et al. 2000; Valentine et al. 2001; Dasgupta and Weitz 2005).

Trajectories obtained by tracking the motion of particles in heterogeneous microenvironments can result from a complex combination of several contributing factors, which influence the trajectory's form (Fig. 1). In addition to naturally occurring thermally-driven diffusion, convective processes may exist due to flow driven by pressure gradients or molecular motors in live cells. This superposition of modes of motion resulting from different physical mechanisms obscures the mechanical and structural characteristics of each one, which are needed to characterize the liquid microenvironment. Hence, accurately quantifying each underlying mode is a key challenge. Particle motion is affected by: the viscoelastic nature of the liquids, interactions with molecules and supra-molecular structures, and external forces, such as gravity, forces applied by laser- or magnetic-tweezers, molecular motors, and pressure gradients. For example, a particle may undergo Brownian diffusion within a spatial confinement that is moving relative to its original location. In biophysical terms, this could delineate a molecule diffusing within the nucleus of a live cell while the entire cell is crawling on the substrate. Here, both the particle motion within the cage and the relative cell motion are of interest, describing inner structure as well as cell motility.

Accurate isolation of the various components of motion is essential for correct analysis of transport and rheological properties and their correlation to structural features. An accepted method is two-particle microrheology, which has been used to eliminate bulk convection (Mason et al. 1997b) and later also examine spatially inhomogeneous materials (Crocker et al. 2000) in a more sophisticated form. By examining the relative thermal motion of two closely-located particles, the relative displacement of the particles averages to zero and bulk rheological properties can be determined. However, this method is limited because it requires the particles to be closely located so that they are in the same microenvironment, and thus are under the influence of the same mechanisms.

External forces acting on micro-scale probe particles have been used to characterize the mechanical properties of stiff micro-structures, such as microtubules and actin (Bausch et al. 1998; Bursac et al. 2005), DNA (Haber and Wirtz 2000), and polymeric materials (Helfer et al. 2000). Trapping of particles in a specific location, for example, by optical tweezers, and study of their thermal fluctuations can provide information about the liquid microenvironment (Addas et al. 2004). Conversely, actively applied forces have not been used to probe liquid microenvironments, because the forced, or directed motion masks the thermal fluctuation driven component, indicative of the liquid properties. Molecular-motor based transport in cells falls under this category. Accurate separation of the components of a trajectory that are thermal or active would allow studies of both mechanisms.

Another common difficulty in particle trajectory analysis is when different short- and long-time scale modes of motion are of interest. The standard approach of analyzing a trajectory by examining the time-dependent displacements on the total trajectory contour length leads to incorrect information in intermediate time-scales, because of superposition of different processes. Hence, isolation of the processes occurring in each time-scale could provide improved information thereby allowing accurate analysis of different time- and length-scale processes in the same trajectory.

Here we present simulations that facilitate the isolation and examination of concurrent modes of motion. Using computer simulations, we qualitatively emulate complex trajectories that have been obtained experimentally with control-parameters such as particle size, viscosity, and temperature as well as characteristic microdomain sizes and convective speeds. By correlating the conditions of the simulated trajectories with experimental ones, structural and physical elements obscured by superposition can be elucidated. For example, the trajectory of a particle undergoing Brownian diffusion while transported on a molecular motor can be separated into passive and active elements, characterizing the liquid microenvironment and the molecular motor velocity. Changing the basic analysis of particle trajectories will consequently affect calculations of rheological properties, such as the material compliance (Xu et al. 1998; Mason 2000) and the elastic and viscous moduli (Mason 2000; Dasgupta et al. 2002).

The structure of this article is as follows: we first describe the design of computer simulations and define the basic modes of motion. Those will serve as building blocks for complex processes. We then generate trajectories and show their qualitative agreement with

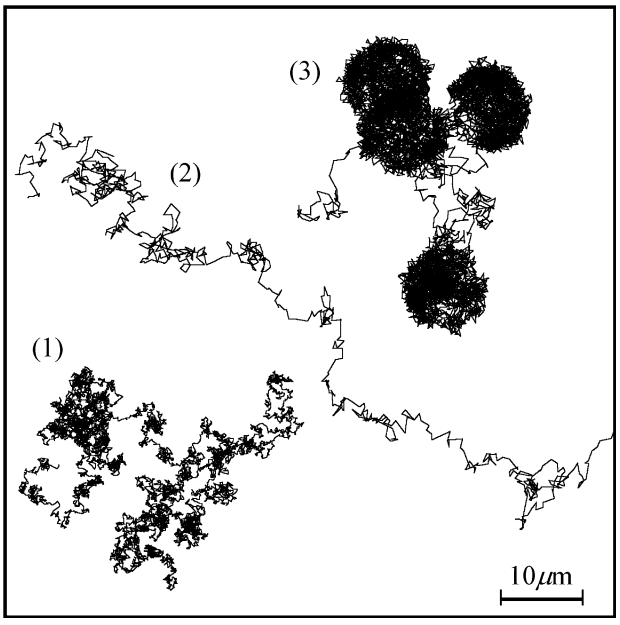

Fig. 1 Trajectories of various types of 50 nm radius particle motion, simulated at a frame rate of 30 Hz: *1* Brownian motion in liquid with viscosity 10× water at 37°C, for consistent scaling; *2* Brownian and convective, directional motion in water at 37°C; *3* Brownian motion, diffusion with transient trapping, and 'escape' by diffusion with convection in water at 37°C

experimental data obtained by others, hence validating the simulations. We introduce some concerns and difficulties in complex trajectory analysis and provide a possible new procedure. Finally, we discuss the implications of this work to experimental particle tracking, data collection and analysis. In-depth discussions of particle tracking (Qian et al. 1991; Saxton and Jacobson 1997) and microrheology (Gardel et al. 2005) methods and background are available elsewhere.

2 Simulation design and parameters

We have created a generic mathematical module that generates 2-dimensonal trajectories of spherical particles in a viscous liquid. We designed the simulations to provide 2-D trajectories that can ultimately be compared to those obtained experimentally by light- or fluorescence-microscopy. We base the trajectory simulations on three basic modes of motion: unconstrained Brownian, spatially constrained, and convective motion, and their combinations. While Brownian and constrained motion are thermal-fluctuation driven, convective motion is obtained experimentally by externally applied forces or molecular motors.

We introduce Brownian motion as the basis of our simulations and establish it as a background process in each experiment. Brownian motion is ergodic, and random in direction and characterized by a Gaussian distribution where the average distance traveled is statistically zero. The displacements in x or y directions of 2-D Brownian motion can each be described by an independent 1-D Gaussian distribution. For our model, we use a built-in function in Matlab 7.0 (Mathworks Inc., Natick, MA) to generate a Gaussian distribution with a mean of 0 and a variance of 1.6. Here the mean is 0, but the mean of the absolute values is 1 and is indicative of a single 1-D step. These distributions serve as a non-dimensional representation of particle-center displacement normalized by an average 1-D step size for each direction. For a given short observation time, t, the distance traveled in a viscous liquid is determined by the diffusion coefficient, D, which is a measure of how rapidly particles move through a fluid at rest. Hence, the square of the distance traveled or the probable step-size in 1-D is (Einstein 1956):

$$\langle \Delta x^2(t) \rangle = \langle \Delta y^2(t) \rangle = 2Dt = \frac{k_B T}{3\pi a \eta} t. \quad (1)$$

The diffusion coefficient $D = k_B T/6\pi a\eta$ depends on the particle radius, a, the liquid viscosity, η, and the temperature, T, and Boltzmann's constant, k_B. The step size or mean square displacement (MSD) in 2-D, $\langle \Delta r^2(t) \rangle = \langle \Delta x^2(t) \rangle + \langle \Delta y^2(t) \rangle = 4Dt$ is usually used to describe the time-dependent dynamics of particle motion.

We now define time-scales that govern complex processes in a diffusive system and the theoretical frame-rates required for their study, neglecting hydrodynamic interactions. We begin by examining the end-to-end distance traveled by a Brownian particle, d, during a given time, t_d. The average size of a single 2-D step that the particle takes $\sqrt{\langle \Delta r^2(t_{\text{frame}}) \rangle}$ is determined by the time per frame, t=t_{frame}, in Eq. 1. Thus, the distance d is approximated by multiplying the square root of the number of steps taken, t_d/t_{frame}, by the length of an average step:

$$t_d = \frac{d^2}{\langle \Delta r^2(t_{\text{frame}}) \rangle} t_{\text{frame}} = \frac{3\pi\eta a d^2}{2k_B T}. \quad (2)$$

The theoretical time per frame (t_{frame} in Eq. 2) defines the inverse of the theoretical frame rate and $\langle \Delta r^2(t) \rangle$ is the average 2-D step-size squared taken during time t. The length d can be the smallest feature studied in the sample and t_d becomes an indication of the frame rate needed for the simulations. Feature size, or d, determines the size of the particle that can be

used to study it. A particle larger than the feature size will provide an estimate of the bulk local rheology, while a particle smaller than the feature size can become entrapped and provide dynamics and structural characteristics of the microdomain (Valentine et al. 2004). The time-step defines the distance traveled in a single frame (Eq. 1). Thus, t_{frame} at specific system conditions, a, η, and T, must be smaller than t_d to prevent the particle from taking steps larger than the feature. In addition, a time step smaller than the characteristic time is necessary to allow fast dynamics, e.g., Brownian motion, to be accurately probed. Hence, for probing fast-dynamics and small features we choose the time-per-frame, or the inverse of the theoretical frame-rate, to be at least two orders of magnitude smaller than the characteristic time.

Another aspect that must be considered is the necessary trajectory length. For accurate interpretation of long time-scale information a temporally longer trajectory, or longer experimentally captured video is needed. That is because the $\langle \Delta r^2(t) \rangle$ becomes statistically unreliable within the last decade in time, where few values averaged. Hence, the trajectory length required to accurately study long time-scale features is approximately $1{,}000t_d$, so that the last decade may be discarded and two decades of information remain to provide good statistics. Thus, in the simulations, the number of captured frames should be extended at a specified frame-rate, or the frame rate should be reduced at a constant number of frames. We kept the number of frames constant and changed the theoretical frame rate to accurately quantify the feature parameters.

In physical systems, particle motion may become non-diffusive as a result of spatial constraints, such as the presence of the cell membrane, or convective motion resulting from molecular motors or externally-applied forces. In non-diffusive transport or in diffusive transport in viscoelastic media, the $\langle \Delta r^2(t) \rangle$ becomes non-linear with time, as other processes are concurrent with naturally-occurring Brownian diffusion. Consequently, the diffusion coefficient is no longer relevant. In many biologically relevant, non-diffusive cases the MSD develops a power-law dependence on the time $\langle \Delta r^2(t) \rangle \sim t^{\alpha}$ (Saxton and Jacobson 1997). The so-called diffusive exponent, α, which is the slope in a log–log plot of $\langle \Delta r^2(t) \rangle$, describes the mode of motion a particle is undergoing and is defined for physical processes between $0 \leq \alpha \leq 2$. An $\alpha = 1$ describes pure diffusion, $0 < \alpha < 1$ indicates spatially confined or subdiffusive motion, and $1 < \alpha < 2$ denote active convection or directed motion. The boundary values of $\alpha = 0$ and $\alpha = 2$ define local elastic trapping and purely convective or ballistic motion, respectively.

Spatial constraints have been added to simulate conditions of local ''caging'' or trapping, which model for example cavities in the meshwork of the cytoskeleton of a cell where a particle may become trapped. Brownian motion has been defined in the background of this process and is visible at time-scales at least an order of magnitude smaller than t_d. Local ''cages'' have been defined as a circular barrier with no preference for any location within them, in effect creating a 'hard trap'; however, the functional form of the MSD is similar to that of a harmonically bound Brownian particle (Mason et al. 1997c; Cheng et al. 2002). Edge encounters result in a random step size forced towards the center. The directionality of rebound has been defined by choosing ±10° relative to the line connecting the current position with the center. This ensured that the particle would re-enter the confinement in no more than three to four steps. The particle distance from the center of the cage is defined as the particle centroid location plus the particle radius, to account for the particle size, as the generated positions are actually locations of the particle centroid. We defined two types of cages: one with ''flexible edges'' where a particle may cross the edge by a few steps, as defined above, resulting in variable distance traveled outside of the cage. The second trap has stiff edges. The flexible cage is representative of soft materials, such as surfactant and cellular microstructures, while the stiff cage simulates solids.

We have also examined cases where a particle undergoes convective, directional motion. Convective motion may result from molecular-motor mediated transport, local application of laser- or magnetic-tweezers, or external temperature gradients. We define the speed and direction of motion, but not the specific driving mechanism, to be able to use the model for various situations. The convective motion has been simulated as occurring in user-defined constant speed and a single direction and concurrent with Brownian motion. This motion is typical, for example, of molecular motor mediated transport (Feneberg et al. 2001). Hence, speeds in the simulation have been chosen around the range of molecular motors, typically between 0.5 and 4 μm/s (Fisher and Kolomeisky 1999; Lindemann 2003).

To correctly define the time scales that govern convective motion, we examine the dimensionless Péclet number, Pe, (Bird et al. 2002) of these processes. The Pe number is the ratio of the speed of convection to the speed of diffusion. Choosing the characteristic length as the average, squared 1-D Brownian distance traveled at a particular time step t, $\langle \Delta x^2(t) \rangle$, and using Eq. 1, we obtain for a convective speed v:

$$\mathrm{Pe} = \frac{v_{\mathrm{convection}}}{v_{\mathrm{diffusion}}} = \frac{v}{D\Big/\sqrt{\langle \Delta x^2 \rangle}} = v\sqrt{\frac{2t}{D}} = v \cdot \sqrt{\frac{12\pi\eta a t}{k_{\mathrm{B}}T}}. \tag{3}$$

The Pe number typically indicates a diffusion-controlled process when Pe < 0.1, a convection-controlled process when Pe > 10, and similar contributions of convection and diffusion for intermediate values. Here, the Pe number determines when motion will appear consistently directional and Brownian motion will be masked.

In the simulations described above, changing the system parameters in Eq. 1 affects the average step size and the form of the trajectory in non-Brownian cases. Trajectories are generated non-dimensionally and dimensionality is added later, hence, no effect on the form of a Brownian simulation is expected. However, in the simulations where the user supplies dimensional spatial confinement size and speed of convective motion, the nature of the trajectory is affected in addition to the basic Brownian step size.

We have combined the three basic modes of motion to generate trajectories of particles diffusing, diffusing and being transiently trapped in cages, and escaping from the cages by diffusion with convection (trajectory 3 in Fig. 1). In this simulation all three processes, diffusion, confinement, and convection occur on the same time-scales. Thus, quantitative analysis of each mode of motion, to obtain the convective speed and cage size, becomes difficult. The simulated particles diffuse within a flexible-edge cage for a randomized time longer than $10t_d$, where d is the trap radius, to allow particles to appear fully trapped and provide good MSD statistics for trap size calculations. Subsequently, particles escape by convection concurrent with Brownian motion at a constant convective speed and random direction in each cycle. Convective regimes have been simulated as short as compared to the trapping, and are a small part of the total trajectory.

Using the three basic modes of motion and their combinations, we have studied the effects of spatial confinements and convective motion. Trajectories have been generated in Matlab 7.0 and the $\langle \Delta r^2(t) \rangle$ was found and analyzed using a separate subroutine (subroutines are available on request from the communicating authors). We have chosen the basic theoretical frame rate at 30 Hz, a typical rate provided by commercial cameras used for tracking fluorescent-particle motion. We have limited our experiments to one, biologically relevant, condition of particle motion in water at 37°C for simplicity. We have chosen the particle size to be 50 nm radius as such particles have been used to study microdomains within live cells (Bacher et al. 2004; Kole et al. 2004).

3 Results and validation

A freely diffusing particle moves in a random direction with Gaussian-distribution step size, which leads to a diffusive exponent of 1 at all time-scales. Figure 2 provides the simulated trajectories of 50 nm radius particles undergoing free diffusion in water at 37°C. Four representative trajectories are presented in Fig. 2a; note that the randomness of the traces is not always evident (see specifically trace 2 in Fig. 2a). The trajectories presented here are comparable to the ones observed experimentally (Mason et al. 1997a; Apgar et al. 2000; Goodman et al. 2002; Suh et al. 2004). The MSDs of the four particles in Fig. 2a are provided in linear and logarithmic representations in Fig. 2b, c, respectively. Note how at longer lag-times, divergences between the curves are evident and the last decade in time of data (>30 s in Fig. 2) is statistically irregular. It is good practice to exclude such data from further consideration due to statistical uncertainty. We also ensemble averaged ten trajectories (Fig. 2d), which provided improved stability at longer lag-times. The $\langle \Delta r^2(t) \rangle$ exhibits a log-slope, or diffusive exponent of 1 for the $\langle \Delta r^2(t) \rangle$ (Fig. 2d) in full agreement with Eq. 1.

When a spatial constraint is applied to a Brownian particle, it diffuses freely until it encounters an edge, resulting in a bounded trajectory. The simulated trajectories of Brownian particles diffusing within flexible edge, circular cages of various sizes are given in Fig. 3a. Trajectories were obtained at varying frame rates according to Eq. 2 and step-size per frame changed inversely with the rate (Eq. 1). The time evolution within three traps of different sizes shows the underlying Brownian motion at the shortest times. Similar trajectories have been observed in experiments, where the Brownian motion was not always apparent at short time-scales (Apgar et al. 2000; Yamada et al. 2000; Tseng et al. 2002; Panorchan et al. 2004), as frame rates may not have been fast enough. The ensemble-averaged $\langle \Delta r^2(t) \rangle$ of ten trajectoried for each of the three cage sizes are given in Fig. 3b, where the different starting times and trajectory lengths are the result of the changing frame rate. The diffusive exponent of 1 is indicative of Brownian motion within the cage before $t_d/10$, while the diffusive exponent of 0 at longer times than t_d represents elastic trapping (Cheng et al. 2002). Simulations were initiated at the center of the cage,

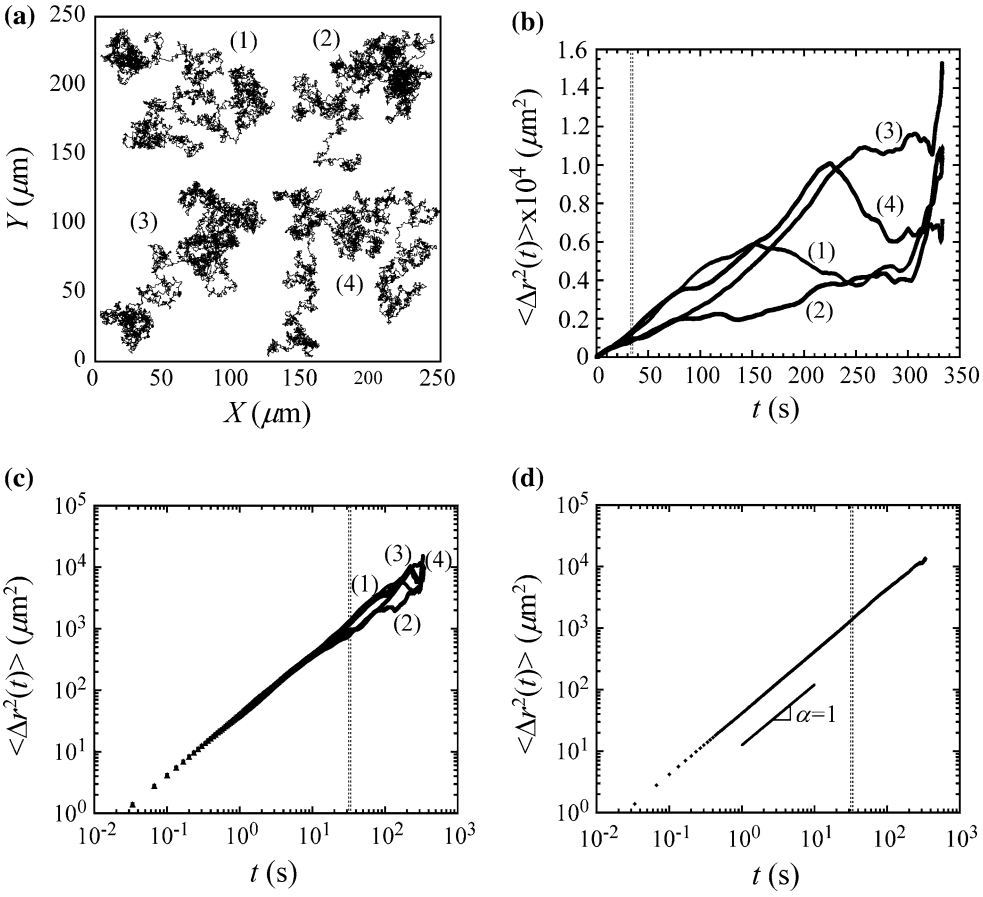

Fig. 2 Simulated trajectories of spheres of radius 50 nm exhibiting thermal-fluctuation mediated diffusive, Brownian motion in water at 37°C. Trajectories were generated at 30 Hz and are 10,000-frames long. **a** Four trajectories of freely diffusing particles. **b** Time-averaged MSD, $\langle \Delta r^2(t) \rangle$, of each trajectory as a function of lag time on a linear scale. Note variations at longer times, *dashed line* indicates data reliability cutoff. Data at longer time-scales is statistically unreliable. **c** Time-averaged MSD of each particle plotted on a log-log plot. **d** Ensemble- and time-averaged MSD of ten similar trajectories. The log-slope, or diffusive exponent of $\alpha = 1$ is indicative of Brownian motion. Ensemble averaging reduces the statistical noise at longer time scales

thus d in Eq. 2 is the cage radius, which is also the average distance in a circular cage regardless of the start point. Similarly, the time to travel this distance, t_d is approximated by the lag-time when the slope changes of the $\langle \Delta r^2(t) \rangle$ from 1 to 0, indicating a change from Brownian motion to local elastic trapping.

We examined the caging process to obtain quantitative correlations for particle trapping events in general. We studied the motion of 50 nm radius Brownian particles within cages between 100 nm and 20 μm in radius, choosing the upper limit on the order of the size of a cell. In smaller traps, Brownian motion has only been observed when theoretical frame-rates were increased significantly, or step sizes reduced according to Eq. 1. The simulated trajectories for all trap sizes were qualitatively similar to those in Fig. 3a. The time to reach the cage edge, t_d where d is the trap radius, has been found by the intersection of the asymptotes to the log-slopes of 1 and 0 on the $\langle \Delta r^2(t) \rangle$. These times were directly proportional to the square of the cage radius and consistent with the values calculated from Eq. 2. Similarly, the plateau MSD ($MSD_{plateau}$) is directly proportional to the cage radius squared (Fig. 3c). The cage radii can be approximated by the root of the $MSD_{plateau}$ plus the particle radius, as in the simulation design and in agreement with previous work (Tseng et al. 2004). Cage radius estimates were consistently larger for flexible cages as compared to stiff cages, as a result of particles stepping out of the cage confines; however, differences were not statistically significant, and in both cases gave an accurate estimation of the cage radius.

A particle diffusing through liquid may become actively transported, for example, by a local flow field, externally applied force, or attachment to a molecular motor. Convective motion has been added to the simulations via predefined speed and direction, chosen form 0.05 to 10 μm/s and direction of 30° relative to the horizon. As the convective speed increased, the Brownian motion of the particles became masked (Fig. 4a). Such trajectories have been observed in solution (Cohen and Moerner 2005) and on cell surfaces during cytoskeletal remodeling (Bursac et al. 2005). When $Pe > 0.1$ according to Eq. 3, directionality becomes apparent and consistent and motion appears convective, $\alpha > 1$. However, motion only becomes fully convective, $\alpha = 2$, at all examination times when $Pe > 10$. Hence, the transition to convective motion,

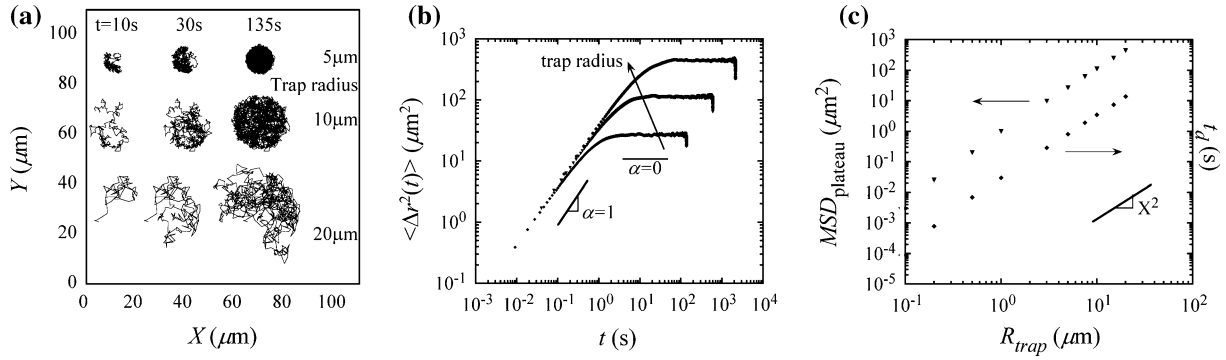

Fig. 3 Simulated trajectories of 50 nm radius spheres diffusing within a flexible-edge circular trap containing water at 37°C. Trajectories were 15,000-frames long. **a** Time-evolution of the trajectories of particles diffusing within cages. Trajectories were produced at frame rates of: 110 Hz for 5 μm radius trap, 25 Hz for 10 μm, and 7 Hz for 20 μm according to Eq. 2. Note how for large cages the confinement is observed in the trajectory only after long times. **b** Ensemble-averaged MSD of ten similarly trapped particles within each cage size. Diffusive exponent of $\alpha \sim 0$ at long times is indicative of local trapping. Initial slope of the MSD ($\alpha = 1$) indicates short time-scale Brownian diffusion within the local trap. **c** Time of confinement impact on the trajectory, t_d, and plateau MSD as a function of the cage radius. Note that both parameters follow a power law of 2 with the cage radius. Theoretical frame-rate for each cage size were chosen as: 0.1 μm radius trap, 1 MHz; 2 μm, 120 kHz; 0.5 μm, 13 kHz; 1 μm, 3 kHz; 3 μm, 300 Hz; 5 μm, 110 Hz; 7.5 μm, 50 Hz; 10 μm, 25 Hz; 15 μm, 12 Hz; and 20 μm, 7 Hz. Error bars are small and not visible on this scale

$\alpha > 1$, occurs at shorter lag-times when the convective speed is larger and other parameters in Eq. 3 are kept constant (Fig. 4b). In addition, when Pe > 0.1, the motion changes from diffusive to ballistic, $\alpha = 2$, while for Pe < 0.1 motion only becomes convective, $\alpha > 1$. Hence, transition times from diffusive to convective cannot be compared for the cases shown in Fig. 4, as the final mode of motion for each speed or Pe is different.

We also examined particles that undergo cycles of trapping and convective escape. Particles were simulated as intermittently diffusing in a 5 μm radius flexible trap and escaping by diffusion superposed on convection at 3 μm/s in a randomized direction, each cycle (Fig. 5a). Trajectories were generated 30,000 frames long at 110 Hz to match conditions in Fig. 3. Trapping regimes are 54.5 to 68 s long and the convective regimes are 4 to 8 s long. The resulting trajectories were similar to data that has been experimentally obtained by us (unpublished data) and others (Weeks et al. 2000; Mizuno et al. 2004; Suh et al. 2004). Standard analysis of the entire trajectories in Fig. 5a produces an ambiguous and misleading $\langle \Delta r^2(t) \rangle$, which were similar up to the reliability cutoff in all cases (Fig. 5b, c). Diffusive motion is observed at short time scales ($\alpha = 1, t < 1$ s) with a change to subdiffusive motion ($\alpha < 1$) between 1 and 10 s followed by another change back to predominantly diffusive motion. Convective motion is not apparent here as the segments are too short to impact the MSD. The alterations in slope indicate possible changes in mode of transport at the corresponding time scales; however, it is unclear what these local slope changes may indicate, as trapping and convection are not clearly depicted by a $\alpha \rightarrow 0$ and $\alpha > 1$, respectively (see Fig. 3b, 4b).

We therefore apply a more sophisticated and practical approach for trajectory analysis, involving segmentation of the data by apparent mode of motion. The simulations in Fig. 5 have been designed so that they are comprised of intermittent regions of diffusion within local traps and escape from the traps via diffusion and convection. Hence, the times of trapping and escape are exactly known and segmentation by mode of motion is straightforward. However, for generalization we have visually defined regions of trapping and escape by the trajectory in Fig. 5a and recalculated the MSD for each mode of motion (Fig. 5d). Segmental analysis and ensemble averaging of the trapping regions (Fig. 5d) reveal that particles diffuse within the traps ($\alpha = 1$) and then become fully trapped ($\alpha = 0$) at times longer than t_d for these conditions. In addition, the square root of the plateau MSD in Fig. 5d plus the particle radius provides an approximation of the trap size 5.27 ± 0.05 μm, a slight overestimation resulting from cage flexibility. Examination of the convective regimes of the trajectory (Fig. 5d) revealed the diffusive nature of the motion at short time scales and convective, $\alpha \sim 2$, at longer time scales.

4 Discussion

We have presented simulations that generate trajectories resembling those in experiments. Using a random number generator and introducing physical

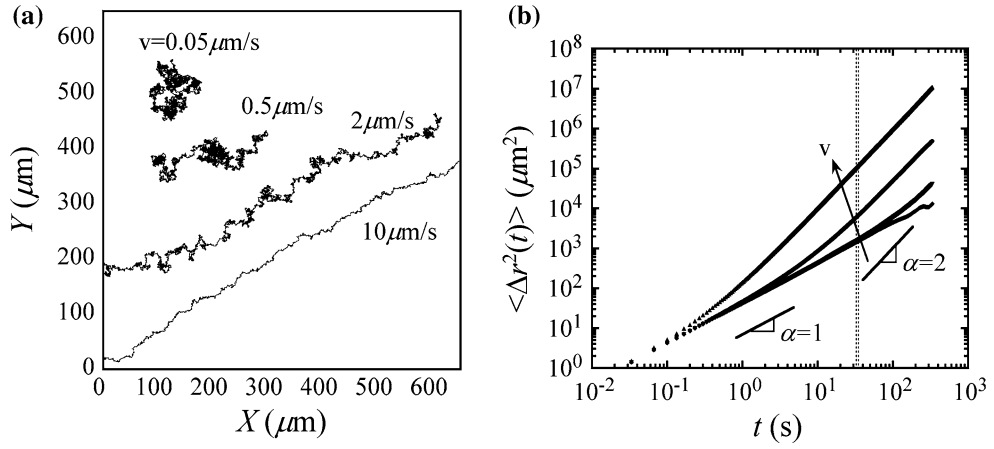

Fig. 4 Simulated trajectories of 50 nm radius particles exhibiting convective motion concurrent with Brownian motion in water at 37°C. Trajectories are generated 10,000-frames long at 30 frames per second. **a** Four trajectories of particles transported at 30° relative to the horizon. Convection speeds are 0.05, 0.5, 2, and 10 μm/s. Only the first 73 s of the fastest moving particle are visible. **b** Ensemble averaged MSD of ten particles for each speed. Diffusive exponent of $\alpha = 1$ is indicative Brownian motion at short lag-times and $\alpha = 2$ at long time scales indicates directed, convective motion

parameters, such as the liquid viscosity, Brownian motion has been generated as the basis and the background motion for each of the processes. We introduced spatial confinements indicative of local particle caging within a sample, showing that particles diffuse freely until encountering edges and trajectories become biased subsequently. In addition, we have examined the effects of convective elements on a particle diffusing through solution. That introduced a directional component affecting the trajectories random nature. The corresponding MSDs of the trajectories obtained here are characteristic of physical processes, adhering to power-laws, indicative of diffusive, subdiffusive, or convective motion.

We have defined characteristic time-scales for confined motion (Eq. 2), which are applicable to experimental systems as well as simulated ones. We observe that for spatial confinements a characteristic time-scale, t_d, exists above which the motion becomes elastically trapped, with a plateau MSD. The characteristic time serves as an indication for the cage size (Eq. 2), which can be used to quantify sizes of cages or confined microdomains within a sample. In addition, t_d also provides a criterion for the frame rate, $1/t_d$, and trajectory length needed to probe different length scales, $1{,}000t_d$. Confined-motion simulations are successful as long as the size of a spatial constraint is larger than a single step size under specific system conditions. According to Eq. 2, if d is smaller than Δx^2, a high frame rate must be chosen to compensate, or the simulations will produce non-physical trajectories. Similarly, in systems where the viscosity is low, or particle is small (Eq. 2), as in the cases illustrated here, short time-scale processes, e.g., Brownian motion, occurring at times shorter than t_d may not be observed unless high frame rates are obtained. Those frame rates, e.g., thousands of frames per second, may be obtained with specialized cameras only. Hence, in experiments where motion appears ''trapped'' at all studied time-scales, short time-scale motion may simply be missed.

The characteristic length scale of confinement, or cage size, can be found when particles become fully trapped. When the shape of the local confinement is circular, one can estimate the trap size from the square root of the plateau value of the MSD at $t > t_d$ plus the particle radius. Flexible edged-cages allow particles to move slightly outside of the boundary, which results in a larger $\mathrm{MSD}_{\mathrm{plateau}}$ and an overestimation of the calculated trap radius, depending on the distance traveled out of the trap. By defining the $t_{\mathrm{frame}} = t_d/100$ (Eq. 2) in all the simulations, we kept the distance a particle may travel outside of the trap approximately constant. Thus, the deviation of the calculated radius from the actual radius remained constant at about 5%. In comparison, when the cages are stiff, the calculated radius is statistically similar to the predefined radius.

Convective motion has previously been limited in analysis, and has simply been categorized as $\alpha > 1$. That has been because separating the convective element from any underlying motion was not possible. We have presented simulations that are composed of directional, convective motion as models for actively transported particles. We suggest that those simulations can aid in accurately separating directed motion, such as that produced by molecular motors or cell

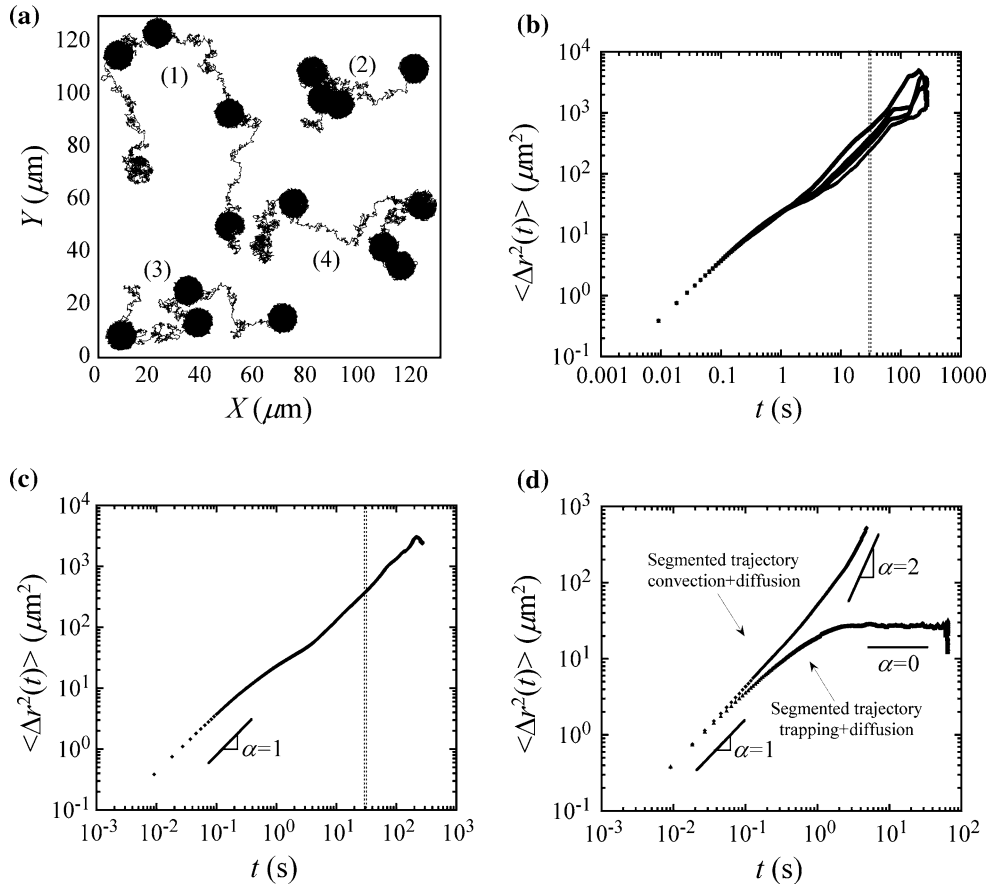

Fig. 5 Simulation of trajectories of spherical particles of radius 50 nm exhibiting cycles of trap and escape by convection in 5 μm radius circular traps in water at 37°C. Convection is 3 μm/s and the direction is randomized in each cycle. Generated trajectories are 30,000-frames long at 110 frames per second. **a** Four trajectories of particles undergoing trap-and-escape motion. The time spent in traps is randomized between 54.5 and 68 s followed by 4 to 8 s of convective motion concurrent with diffusive motion. **b** MSDs of the four trajectories in (**a**). *Dashed line* indicates cutoff of statistically reliable data. **c** Ensemble-averaged MSD of the entire trajectories. Particles are undergoing Brownian diffusion at short time-scales $\alpha = 1$. *Dashed line* indicates cutoff of statistically reliable data. **d** Ensemble averaged MSD of trapped- and convective-motion segments only. Note that segmental analysis allows detection of full trapping ($\alpha = 0$) and convection ($\alpha > 1$) at long times scales, as well as diffusive motion ($\alpha = 1$) at short times

motility, from thermally-induced particle motion. By generating simulations that closely resemble experimental results, the convective speed and directionality as well as the liquid viscosity can be obtained, allowing both processes to be studied simultaneously.

Analysis of complex processes, such as the trap-escape simulation in Fig. 5, require specialized approaches, as standard procedures fail to provide accurate details. We applied visual segmentation by mode of motion as an alternative. Typically, the $\langle \Delta r^2(t) \rangle$ of an entire trajectory of a single particle is found. After that, several particles may be ensemble averaged to provide better statistics. However, obtaining the MSD of an entire trajectory may obscure the physical implication when complex processes are occurring. Close comparison of Fig. 5c, d shows that the same information was initially present, albeit inaccessible in the standard whole-trajectory analysis. The time at which the transition from diffusion to trapping occurs in Fig. 5d is about 1 s, similar to the transition between subdiffusion and diffusion in Fig. 5c. Also, the longest time in a trap (about 68 s) is close to the time at which the motion becomes diffusive again in Fig. 5c. Hence, quantitative information about each concurrent mode of motion is present in Fig. 5c, but is difficult to accurately quantify.

Segmentation of the trajectory becomes more difficult when experimental data is addressed. For the simulations, it is straightforward to separate the trapping from the convective regimes, as we simulate for predefined times and modes of motion clearly visible in the trajectories. However, in experiments as well as some simulations (see particle 2 in Fig. 5) traps can also be close together making their visual separation

difficult. Such a trajectory can also indicate dynamics of the local trap or axis motion, e.g., a cell crawling on the surface or flow driven motion of the entire sample, making distinction between several overlapping traps and one 'stretched' trap difficult. Hence, generalization and automation of the segmentation analysis for ambiguous trajectories could improve understanding of the physical processes and their structural significance.

In the future, more levels of complexity can be added to the simulations. This includes making the liquid viscoelastic to more accurately describe crowded microenvironments in cells. Also, more complex combinations of the basic modes of motion will be studied and automation of their analysis will be addressed, e.g., automated segmental trajectory-analysis of trap-escape data. These simulations may also be extended to provide 3-D trajectories, which would replicate conditions available by confocal microscopy.

Particle tracking can be used to find rheological properties of liquid microenvironments and strength and fluidity of soft-solids. The methods we presented here allow more accurate analysis and interpretation of experimental data. Quantitative mapping of regions within a sample provides an indication of the samples' mechanical responses and through them the functional properties. Hence, accurate analysis of particle tracking data can help provide correlations between structure and function.

Acknowledgements Supported by National Institute of Health grants PN2EY018228-01, CA90571, CA107300, and GM073981 and CMISE, a National Aeronautics and Space Administration URETI Institute Award NCC 2-1364. M.A.T. is a Scholar of the Leukemia and Lymphoma Society. T.G.M. is supported by the American Chemical Society PRF 42858-AC7.

References

Addas KM, Schmidt CF, Tang JX (2004) Microrheology of solutions of semiflexible biopolymer filaments using laser tweezers interferometry. Phys. Rev. E 70:Art. No. 021503

Apgar J, Tseng Y, Fedorov E, Herwig MB, Almo SC, Wirtz D (2000) Multiple-particle tracking measurements of heterogeneities in solutions of actin filaments and actin bundles. Biophys J 79:1095–1106

Bacher C, Reichenzeller M, Athale C, Herrmann H, Eils R (2004) 4-D single particle tracking of synthetic and proteinaceous microspheres reveals preferential movement of nuclear particles along chromatin-poor tracks. BMC Cell Biol 5:45

Bausch AR, Ziemann F, Boulbitch AA, Jacobson K, Sackmann E (1998) Local measurements of viscoelastic parameters of adherent cell surfaces by magnetic bead microrheometry. Biophys J 75:2038–2049

Bausch AR, Moller W, Sackmann E (1999) Measurement of local viscoelasticity and forces in living cells by magnetic tweezers. Biophys J 76:573–579

Bird RB, Stewart WE, Lightfoot ED (2002) Transport phenomena. Wiley, New Jersey

Bursac P, Lenormand G, Fabry B, Oliver M, Weitz DA, Viasnoff V, Butler JP, Fredberg JJ (2005) Cytoskeletal remodelling and slow dynamics in the living cell. Nat Mat 4:557–561

Cheng Z, Chaikin PM, Mason TG (2002) Light streak tracking of optically trapped thin microdisks. Phys Rev Lett 89:108303

Cohen AE, Moerner WE (2005) Method for trapping and manipulating nanoscale objects in solution. Appl Phys Lett. 86:Art. No. 093109

Crocker JC, Grier DG (1996) Methods of digital video microscopy for colloidal studies. J Colloid Int Sci 179:298–310

Crocker JC, Valentine MT, Weeks ER, Gisler T, Kaplan PD, Yodh AG, Weitz DA (2000) Two-point microrheology of inhomogeneous soft materials. Phys Rev Lett 85:888–891

Dasgupta BR, Tee SY, Crocker JC, Frisken BJ, Weitz DA (2002) Microrheology of polyethylene oxide using diffusing wave spectroscopy and single scattering. Phys Rev E 65

Dasgupta BR, Weitz DA (2005) Microrheology of cross-linked polyacrylamide networks. Phys Rev E 71

Einstein A (1956) Investigation on the theory of brownian movement. Dover, New York

Evans E, Ritchie K, Merkel R (1995) Sensitive force technique to probe molecular adhesion and structural linkages at biological interfaces. Biophys J 68:2580–2587

Feneberg W, Westphal M, Sackmann E (2001) Dictyostelium cells' cytoplasm as an active viscoplastic body. Eur Biophys J. Biophys Lett 30:284–294

Fisher ME, Kolomeisky AB (1999) The force exerted by a molecular motor. PNAS 96:6597–6602

Gardel ML, Valentine MT, Crocker JC, Bausch AR, Weitz DA (2003) Microrheology of entangled F-actin solutions. Phys Rev Lett. 91:Art. No. 158302

Gardel ML, Valentine MT, Weitz DA (2005) Microrheology. In: Breuer K (ed) Microdiagnostics. Springer, Berlin Heidelberg New York

Gittes F, Schnurr B, Olmsted PD, MacKintosh FC, Schmidt CF (1997) Microscopic viscoelasticity: shear moduli of soft materials determined from thermal fluctuations. Phys Rev Lett 79:3286–3289

Goodman A, Tseng Y, Wirtz D (2002) Effect of length, topology, and concentration on the microviscosity and microheterogeneity of DNA solutions. J Mol Biol 323:199–215

Haber C, Wirtz D (2000) Magnetic tweezers for DNA micromanipulation. Rev Sci Instr 71:4561–4570

Helfer E, Harlepp S, Bourdieu L, Robert J, MacKintosh FC, Chatenay D (2000) Microrheology of biopolymer-membrane complexes. Phys Rev Lett 85:457–460

Kole TP, Tseng Y, Huang L, Katz JL, Wirtz D (2004) Rho kinase regulates the intracellular micromechanical response of adherent cells to rho activation. Mol Biol Cell 15:3475–3484

Lindemann CB (2003) Structural-functional relationships of the dynein, spokes, and central-pair projections predicted from an analysis of the forces acting within a flagellum. Biophys J 84:4115–4126

Mason TG (2000) Estimating the viscoelastic moduli of complex fluids using the generalized Stokes-Einstein equation. Rheol Acta 39:371–378

Mason TG, Weitz DA (1995) Optical measurements of frequency-dependent linear viscoelastic moduli of complex fluids. Phys Rev Lett 74:1250–1253

Mason TG, Ganesan K, vanZanten JH, Wirtz D, Kuo SC (1997a) Particle tracking microrheology of complex fluids. Phys Rev Lett 79:3282–3285

Mason TG, Dhople A, Wirtz D (1997b) Concentrated DNA rheology and microrheology. MRS proc stat mech phys biol 463:153–156

Mason TG, Gang H, Weitz DA (1997c) Diffusing-wave-spectroscopy measurements of viscoelasticity of complex fluids. J Opt Soc Am A 14:139–149

Mizuno D, Kimura Y, Hayakawa R (2004) Electrophoretic microrheology of a dilute lamellar phase: Relaxation mechanisms in frequency-dependent mobility of nanometer-sized particles between soft membranes. Phys Rev E 70

Panorchan P, Schafer BW, Wirtz D, Tseng Y (2004) Nuclear envelope breakdown requires overcoming the mechanical integrity of the nuclear lamina. J Biol Chem 279:43462–43467

Qian H, Sheetz M, Elson E (1991) Single particle tracking. Analysis of diffusion and flow in two-dimensional systems. Biophys J 60:910–921

Salman H, Gil Y, Granek R, Elbaum M (2002) Microtubules, motor proteins, and anomalous mean squared displacements. Chem Phys 284:389–397

Saxton MJ, Jacobson K (1997) Single-particle tracking: Applications to membrane dynamics. Annu Rev Biophys Biomol Struct 26:373–399

Suh JH, Wirtz D, Hanes J (2004) Real-time intracellular transport of gene nanocarriers studied by multiple particle tracking. Biotech. Progr. 20:598–602

Tseng Y, Kole TP, Wirtz D (2002) Micromechanical mapping of live cells by multiple-particle-tracking microrheology. Biophys. J. 83:3162–3176

Tseng Y, Lee JSH, Kole TP, Jiang I, Wirtz D (2004) Micro-organization and visco-elasticity of the interphase nucleus revealed by particle nanotracking. J Cell Sci 117:2159–2167

Valentine MT, Kaplan PD, Thota D, Crocker JC, Gisler T, Prud'homme RK, Beck M, Weitz DA (2001) Investigating the microenvironments of inhomogeneous soft materials with multiple particle tracking. Phys Rev E 6406:Art. No. 061506

Valentine MT, Perlman ZE, Gardel ML, Shin JH, Matsudaira P, Mitchison TJ, Weitz DA (2004) Colloid surface chemistry critically affects multiple particle tracking measurements of biomaterials. Biophys J 86:4004–4014

Weeks ER, Crocker JC, Levitt AC, Schofield A, Weitz DA (2000) Three-dimensional direct imaging of structural relaxation near the colloidal glass transition. Science 287:627–631

Yamada S, Wirtz D, Kuo SC (2000) Mechanics of living cells measured by laser tracking microrheology. Biophys J 78:1736–1747

Yamada S, Wirtz D, Coulombe PA (2002) Pairwise assembly determines the intrinsic potential for self-organization and mechanical properties of keratin filaments. Mol Biol Cell 13:382–391

Xu JY, Viasnoff V, Wirtz D (1998) Compliance of actin filament networks measured by particle-tracking microrheology and diffusing wave spectroscopy. Rheologica Acta 37:387–398